https://doi.org/10.5194/egusphere-2022-375
Preprint. Discussion started: 30 May 2022

Vertical profiles of cloud condensation nuclei number concentration and its empirical estimate from aerosol optical properties over the North China Plain

Rui Zhang[1], Yuying Wang[1], Zhanqing Li[2,3], Zhibin Wang[4], Russell R. Dickerson[3], Xinrong Ren[3], Hao He[3], Fei Wang[5], Ying Gao[6], Xi Chen[1], Jialu Xu[1], Yafang Cheng[7], Hang Su[8]

[1] Key Laboratory for Aerosol-Cloud-Precipitation of China Meteorological Administration, School of Atmospheric Physics, Nanjing University of Information Science & Technology, Nanjing 210044, China

[2] State Key Laboratory of Remote Sensing Science, College of Global Change and Earth System Science, Beijing Normal University, Beijing 100875, China

[3] Earth System Science Interdisciplinary Center, Department of Atmospheric and Oceanic Science, University of Maryland, College Park, MD, USA

[4] Research Center for Air Pollution and Health, College of Environmental and Resource Science, Zhejiang University, Hangzhou 310058, China

[5] Key Laboratory for Cloud Physics, Chinese Academy of Meteorological Sciences, Beijing, 100081, China

[6] School of Atmospheric Sciences, Nanjing University, Nanjing 210008, China

[7] Minerva Research Group, Max Planck Institute for Chemistry, 55128 Mainz, Germany

[8] Multiphase Chemistry Department, Max Planck Institute for Chemistry, 55128 Mainz, Germany

Correspondence to: Yuying Wang (yuyingwang@nuist.edu.cn)

https://doi.org/10.5194/egusphere-2022-375
Preprint. Discussion started: 30 May 2022

Abstract

To better understand the characteristics of aerosol activation ability and optical properties, a comprehensive airborne campaign was implemented over the North China Plain (NCP) from May 8 to June 11, 2016. Vertical profiles of cloud condensation nuclei (CCN) number concentration (N_{CCN}) and aerosol optical properties were measured simultaneously. Seventy-two-hour air mass back trajectories show that during the campaign the measurement region is mainly influenced by air masses in northwest and southeast. Air mass sources, temperature structure, anthropogenic emissions, and terrain distribution are factors influencing N_{CCN} profiles. CCN spectra suggest that the ability of aerosol activation into CCN is stronger in southeast air masses than in northwest air masses and stronger in the free atmosphere than near the surface. Vertical distributions of aerosol scattering Ångström exponent (SAE) indicate that aerosols near the surface mainly originate from primary emissions consisting of more fine particles. The combined effect of aerosol lifting aloft and long-distance transport increase SAE and make it vary more in the free troposphere than near the surface. For parameterizing N_{CCN}, the equation $N_{\mathrm{CCN}}=10^{\beta}\cdot\sigma^{\gamma}$ is used to fit the relationship between N_{CCN} and the aerosol scattering coefficient (σ) at 450 nm. The fitting parameters β and γ have linear relationships with the SAE. Empirical estimates of N_{CCN} at 0.7% water vapor supersaturation (*ss*) from aerosol optical properties are thus retrieved for the two air masses: $N_{\mathrm{CCN}}=10^{-0.22\cdot\mathrm{SAE}+2.39}\cdot\sigma^{0.30\cdot\mathrm{SAE}+0.29}$ for northwest air masses and $N_{\mathrm{CCN}}=10^{-0.07\cdot\mathrm{SAE}+2.29}\cdot\sigma^{0.14\cdot\mathrm{SAE}+0.28}$ for southeast air masses. The estimated N_{CCN} at 0.7% *ss* agrees with that measured, although the performance differs between low and high concentrations in the two air masses. The results highlight the important impact of aerosol sources on the empirical estimate of N_{CCN} from aerosol optical properties.

1. Introduction

Defined as the mixture of solid and liquid particles suspended in the air, aerosols have a great impact on Earth's climate system via their direct and indirect effects (IPCC, 2021). They not only alter Earth's radiation budget by absorbing and scattering solar radiation directly (e.g., Bond et al., 2013) but also affect the radiation budget indirectly by serving as cloud condensation nuclei (CCN),

https://doi.org/10.5194/egusphere-2022-375
Preprint. Discussion started: 30 May 2022

modifying the microphysical properties of clouds (e.g., Lohmann and Feichter, 2005; Andreae and Rosenfeld, 2008). This is referred to as aerosol-cloud interactions (ACI). Many studies suggest that good knowledge of the CCN activation ability is the key to quantitatively evaluating ACI and its radiative forcing in models (e.g., Rosenfeld et al., 2014, 2016; Z. Li et al., 2016, 2019; Liu and Li., 2020). However, this is uncertain because of the lack of comprehensive observations.

CCN is a subset of aerosols that can be activated at a certain water vapor supersaturation (*ss*). The activation ability is mainly determined by three aerosol properties, namely, particle size, chemical composition, and mixing state (e.g., Farmer et al., 2015; F. Zhang et al., 2017; Cai et al., 2018; Y. Wang et al., 2018). Previous studies have reported that these three factors have large spatiotemporal variabilities over different regions in the world (e.g., Juranyi et al., 2011; Paramonov et al., 2015; Schmale et al., 2018), especially in fast-developing countries like China (Z. Li et al., 2019). This increases the uncertainty of estimates of ACI.

To evaluate the effect of aerosols on air quality and atmospheric radiative forcing in China, many field experiments have been carried out in recent years in some developed regions, such as the Pearl River Delta (PRD) (e.g., Rose et al., 2010), the Yangtze River Delta (YRD) (e.g., Leng et al., 2013), and the North China Plain (NCP) (e.g., L. J. Guo et al., 2015; F. Zhang et al., 2017; J. Ren et al., 2018). Some of these studies including measurements of CCN aimed at investigating the characteristics of CCN activation properties and their influential factors or establishing reasonable estimation schemes for CCN number concentration (N_{CCN}). For example, L. J. Guo et al. (2015) discussed the change in CCN activation properties in a long-lasting severe fog and haze episode. F. Zhang et al. (2017) conducted N_{CCN} closure experiments, finding that N_{CCN} was well estimated using the data of aerosol size number concentration and bulk chemical composition but it was influenced by the aerosol aging level. J. Ren et al. (2018) suggested that it was better to predict N_{CCN} using aerosol size-resolved rather than bulk chemical composition data. However, most of these studies were based on ground-based observations, which could not characterize the vertical distributions of CCN properties and N_{CCN} profiles. The CCN activation ability and N_{CCN} below cloud bases are key in quantifying ACI (Rosenfeld et al., 2014; Z. Li et al., 2016). Therefore, it is necessary to do more studies about CCN profiles in China.

A commonly used platform to observe N_{CCN} profiles and the vertical distribution of CCN activation ability is an aircraft (e.g., J. Li et al., 2015b; Jayachandran et al., 2020a; Manoj et al.,

https://doi.org/10.5194/egusphere-2022-375
Preprint. Discussion started: 30 May 2022

2021; Z. Cai et al., 2022). However, limited by high costs and technological complexity, current aircraft measurements are insufficient to quantify ACI. Some studies have thus attempted to estimate N_{CCN} using aerosol optical data (e.g., Andreae, 2009; Liu and Li, 2014; Tao et al., 2018). For example, Andreae (2009) built an exponential function between N_{CCN} and aerosol optical depth (AOD). Liu and Li (2014) defined the aerosol scattering index (AI) using aerosol scattering coefficients (σ) and aerosol scattering Ångström exponent (SAE) to estimate N_{CCN}. Tao et al. (2018) proposed a new method for estimating N_{CCN} based on a three-wavelength humidified nephelometer system. Most of these N_{CCN} parameterization schemes, however, were conducted based on ground-based observations in different regions and were rarely verified by in situ N_{CCN} profiles.

Over the past few decades, rapid industrialization and urbanization have made the NCP one of the most heavily polluted regions in China. The large number of aerosols and gases emitted by human activities deteriorated air quality, strongly impacting the regional climate (e.g., Fan et al., 2016; Chen et al., 2022). The aerosol activation ability and optical properties in the NCP have drawn much attention (e.g., Zhang et al., 2016, 2017; Wang et al., 2018b). In light of this, we undertook a comprehensive airborne campaign in the NCP under the aegis of a project called Air chemistry Research In Asia (ARIAs). We directly measured profiles of N_{CCN} and aerosol optical properties from an aircraft and analyzed the CCN activation property and relationships between N_{CCN} and aerosol optical properties. This study will provide a perspective to improve aerosol-cloud parameterizations applied in the NCP. Analytical methods developed here will also be applicable to other regions of the world.

This paper is structured as follows. Details about the airborne campaign, instruments, and air mass sources are given in Section 2. Section 3 discusses and analyzes N_{CCN} profiles at 0.7% *ss*, vertical distributions of CCN spectra, and possible relationships between N_{CCN} and aerosol optical properties. Section 4 summarizes the major conclusions of this study.

2. Airborne campaign, instruments, and air mass sources

2.1 Airborne campaign

Hebei province (36°05' N-42°40' N, 113°27' E-119°50' E) is located north of the Yellow River and east of the Taihang Mountains in the NCP. It surrounds the Beijing and Tianjin megacities,

https://doi.org/10.5194/egusphere-2022-375
Preprint. Discussion started: 30 May 2022

and borders Shangdong province to the east, Shanxi province to the west, Henan province to the south, and the Inner Mongolia Autonomous Region to the north (Fig. 1a). The terrain of Hebei province is high in the northwest and low in the southeast, with the altitude generally decreasing from the northwest to the southeast. The plain area covers most of Hebei province, located in the eastern foothills of the Taihang Mountains.

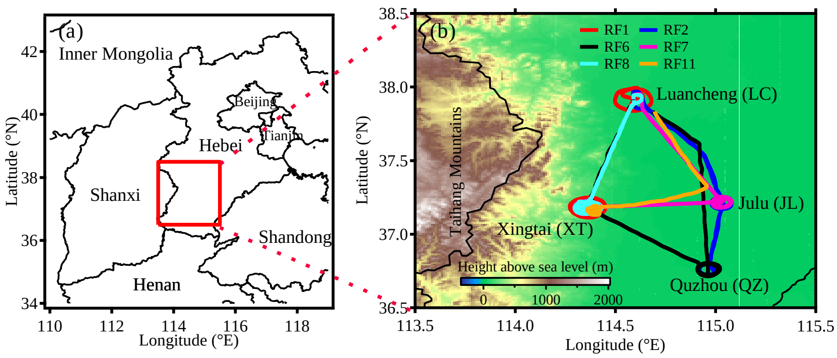

Figure 1. **(a)** The geographic location of Hebei province and **(b)** flight tracks of six flights conducted over the southern plain of Hebei province in from May 8 to June 11, 2016. The colored background shows terrain heights above sea level (unit: m).

The ARIAs campaign was carried out from May 8 to June 11, 2016 in the southern plain area of Hebei province using a Y-12 turboprop airplane operated by the Weather Modification Office of the Hebei Meteorological Bureau. The details of the flight plans were introduced in F. Wang et al. (2018). Luancheng (LC, 114.36° E, 37.18° N; 182 m above sea level, or a.s.l.), Xingtai (XT, 114.36° E, 37.18° N; 182 m a.s.l.), Julu (JL, 115.02° E, 37.22° N; 20 m a.s.l.), and Quzhou (QZ, 114.96° E, 36.76° N; 40 m a.s.l.) are the four central sampling sites (Fig. 1b), all to the east of the Taihang Mountains. Six flights (RF1, RF2, RF6, RF7, RF8, and RF11) measuring N_{CCN} and aerosol optical properties are used in this study. In all the flights, the Y-12 airplane conducted vertical spiral flights from ~0.3 to ~3.5 km near one or two central sampling sites and level flights at different fixed altitudes between different central sampling sites. Every flight obtained several N_{CCN} profiles at one or two sites and N_{CCN} data at several fixed altitudes. Table 1 lists details about the flight tracks (also see Fig. 1b).

Altitudes are distances a.s.l. in this study. All aircraft flights except RF8 (conducted from 16:30–18:24 CST; CST stands for China standard time, which is 8h ahead of UTC) were conducted

https://doi.org/10.5194/egusphere-2022-375
Preprint. Discussion started: 30 May 2022

around noon (10:00–15:00 CST), when the planetary boundary layer (PBL) height was fully developed.

Table 1. Detailed information about the flight tracks deployed during the campaign. Flight code (third column): The number after 'RF' indicates the flight number, the number after '_' indicates the number of vertical spiral flights, and the letter after '_' indicates the number of level flights.

Flight number, date	Time range (CST)	Flight code	Region covered	Vertical height a.s.l. (km)
RF1, 20160508	13:02–14:29	RF1_1	XT	0.3–3.7
		RF1_a	track from XT to LC	~3.6
		RF1_2	LC	0.3–3.2
RF2, 20160515	12:17–15:04	RF2_a	track from LC to JL	~0.4
		RF2_1	JL	0.3–3.6
		RF2_2	QZ	0.3–3.6
		RF2_b	track from QZ to JL	~3.6
		RF2_c	track from JL to LC	~0.4
RF6, 20160521	12:04–14:41	RF6_1	QZ	0.3–3.1
		RF6_a	track from QZ to XT	~2.5
		RF6_2	XT	0.3–2.6
		RF6_b	track from XT to LC	~1.1
RF7, 20160528	10:21–13:25	RF7_a	track around XT	~3.1
		RF7_1	XT	0.5–3.1
		RF7_b	track from XT to JL	~0.4
		RF7_2	JL	0.3–2.5
		RF7_c	track from JL to LC	~1.8
RF8, 20160528	16:30–18:24	RF8_a	track around XT	~0.6
		RF8_1	XT	0.5–3.1
RF11, 20160611	11:07–12:28	RF11_a	track around XT	~0.6
		RF11_1	XT	0.3–3.2

2.2 Instruments

To satisfy the needs of this study, the Y-12 airplane was equipped with a dual-column CCN counter (CCNc), a three-wavelength integrating nephelometer, and a Cloud Water Inertial Probe (CWIP). All instruments were calibrated rigorously prior to the airborne campaign. Table 2 summarizes the instruments equipped on the airplane.

https://doi.org/10.5194/egusphere-2022-375
Preprint. Discussion started: 30 May 2022

Table 2. Instruments equipped on the Y-12 airplane used in this study.

Instrument	Parameter	Time resolution	Accuracy
CCN counter (model CCNc-200, DMT Inc.)	CCN number concentrations（N_{CCN}）	1 s	–
Nephelometer (model 3565, TSI Inc.)	Aerosol scattering coefficients (σ) at three wavelengths (450, 550, and 700 nm)	1 s	0.5 Mm^{-1}
CWIP (Rain Dynamics Inc.)	Temperature (T)	1 s	1 K
	Relative humidity (RH)	1 s	2%
	Position	0.1 s	–

N_{CCN} was measured by a dual-column continuous-flow thermal-gradient cloud condensation nuclei counter (model CCN_C-200, DMT Inc.) with a time resolution of 1 s. It is equipped with two columns that can simultaneously measure N_{CCN} at two different *ss* levels without mutual interference. In this campaign, only one *ss* level is set in the first column during all flights, but eight different *ss* levels are set in the second column with a measurement time interval of 90 s for each *ss* level. Considering the equilibrium time of *ss* levels, the final 30 s data at any *ss* level in the cycle for the second column is used in this study. The *ss* level in columns was calibrated with pure ammonium sulfate following procedures developed by Rose et al. (2008). The *ss* level in the first column was corrected to 0.7% and the *ss* levels in the second column were corrected to 0.44%, 0.56%, 0.68%, 0.80%, 0.92%, 1.04%, 1.16%, and 1.28%. N_{CCN} profiles at 0.7% *ss* and N_{CCN} data at different *ss* levels were thus available.

The integrating nephelometer (model 3565, TSI Inc.) can continuously measure aerosol scattering coefficients (σ) at three wavelengths (450, 550, and 700 nm) with a time resolution of 1 s. Previous studies have shown that σ becomes larger with increasing relative humidity (RH) due to aerosol hygroscopic growth (e.g., L. Zhang et al., 2015; R. Ren et al., 2021). Hence, the RH of sampled air was dried to below 40% in this campaign. The nephelometer was calibrated and tested rigorously prior to the airborne campaign using carbon dioxide gas and filtered zero air. Anderson and Ogren (1998) have provided details about the calibration methods and measurement uncertainties of this nephelometer.

Ambient temperature (T) and RH were measured by a CWIP (Rain Dynamics Inc.) with a time resolution of 1 s during flights. Real-time flight position data such as longitude, latitude, and

https://doi.org/10.5194/egusphere-2022-375
Preprint. Discussion started: 30 May 2022

altitude were recorded by a global positioning system (GPS) and the CWIP with a time resolution of 0.1 s. The CWIP time was calibrated and synchronized with the GPS time prior to deployment.

2.3 Air mass sources

Previous studies have suggested that differences in air masses will lead to spatiotemporal differences in CCN activation ability and aerosol optical properties (e.g., Xu et al., 2020; Jayachandran et al., 2020b). To better understand air mass sources and aerosol transport pathways over the measurement area, seventy-two-hour air mass back trajectories for all N_{CCN} profiles at 0.5, 1.5, 2.5, and 3.5 km are analyzed using the NOAA Hybrid Single Particle Lagrangian Integrated Trajectory (HYSPLIT) model (Draxier and Hess, 1998). Results show that the sampling region is mainly influenced by two distinct air masses, namely, northwest air masses and southeast air masses (Fig. 2). Northwest air masses (Fig. 2a) originate from arid or semi-arid land, including five N_{CCN} profiles whose flight codes are RF1_1, RF1_2, RF2_1, RF2_2, and RF11_1. Before these trajectories approach the sampling area, most of these air masses flow around or are forced to lift due to the influence of the Taihang Mountains. However, southeast air masses (Fig. 2b) originate from coastal or marine areas, also including five N_{CCN} profiles whose flight codes are RF6_1, RF6_2, RF7_1, RF7_2, and RF8_1. Air masses in place during the RF7_1, RF7_2, and RF8_1 flights originate from coastal areas, and those during the RF6_1 and RF6_2 flights originate from the western Pacific. Southeast trajectories pass over the densely populated plain region to the east and south of the sampling area, which is easily impacted by anthropogenic emissions. These trajectories are also easily affected by differences in land and sea thermal properties, raising the air masses gradually before reaching the sampling area (Fig. S1).

https://doi.org/10.5194/egusphere-2022-375
Preprint. Discussion started: 30 May 2022

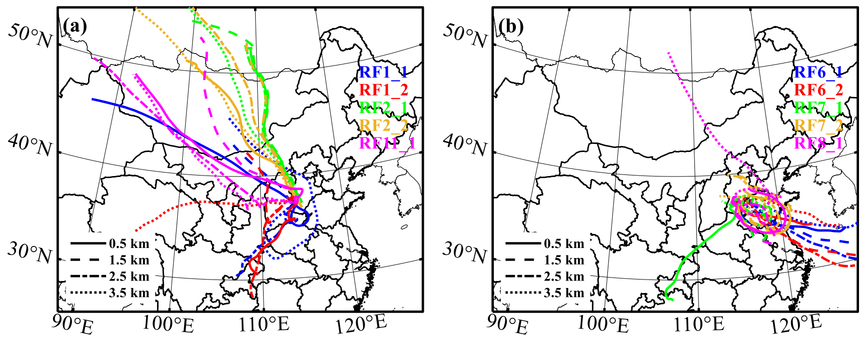

Figure 2. Seventy-two-hour HYSPLIT back trajectories over the sampling region: (**a**) northwest air masses and (**b**) southeast air masses. The color of trajectories indicates different flight codes associated with N_{CCN} profiles. The line type shows trajectories with different starting altitudes (0.5, 1.5, 2.5, and 3.5 km).

3. Results and Discussion

3.1 Vertical distributions of N_{CCN}

3.1.1 Effect of the temperature inversion layer (TIL) on N_{CCN} profiles

Previous studies have demonstrated the significant impact of the TIL structure on the vertical distributions of aerosols and N_{CCN} (e.g., Janhäll et al., 2006; J. Li et al., 2015a, 2015b). Here, N_{CCN} profiles are classified into three categories according to the number of TILs (Table 3). Three typical N_{CCN} profiles at 0.7% *ss* (RF2_1, RF6_1, and RF1_1) with different numbers of TILs are chosen for comparison purposes (Fig. 3; N_{CCN} profiles associated with the other three flight codes are shown in Figs. S2–4).

Table 3. Classification of different N_{CCN} profiles based on the number of TILs.

Categories	Flight codes of N_{CCN} profiles
No TIL	RF2_1, RF2_2
One TIL	RF6_1, RF6_2, RF7_1, RF7_2, RF8_1, RF11_1
Two TILs	RF1_1, RF1_2

No TIL: Figure 3a shows vertical profiles of T and potential temperature (θ) for the RF2_1 N_{CCN} profile (Fig. 3b). T decreases with altitude in the absence of a TIL while the variation in θ with

https://doi.org/10.5194/egusphere-2022-375
Preprint. Discussion started: 30 May 2022

altitude ($\partial\theta/\partial z$) is generally small below ~2.3 km (Fig. 3a). These meteorological conditions are favorable for the upward transport of aerosols below ~2.3 km. The larger $\partial\theta/\partial z$ above ~2.3 km suggests a more stable atmosphere, suppressing the upward transport of aerosols (Yau and Rogers, 1998). This is why N_{CCN} peaks at ~2.3 km and decreases rapidly above (Fig. 3b). However, a second N_{CCN} peak is observed at ~3.2 km, with a small $\partial\theta/\partial z$ in the vicinity. The seventy-two-hour back trajectory shows that the air mass in this case originates from the northwestern arid/semi-arid parts of Mongolia (Fig. 2a). The long-distance transport of aerosols (like dust particles) may be responsible for the N_{CCN} peak at ~3.2 km. In another N_{CCN} profile with no TIL (RF2_2), a weak N_{CCN} peak also appears at ~3.2 km (Fig. S2b). The RF11_1 N_{CCN} profile with similar back trajectories as RF2_1 and RF2_2 also has a weak N_{CCN} peak at ~3.2 km. This suggests that the long-distance transport of aerosols plays an important role in N_{CCN} in the free troposphere over the NCP under the influence of northwest air masses. Note that high N_{CCN} in the free troposphere has an important impact on cloud microphysical properties (Rosenfeld et al., 2008).

One TIL: The temperature profile in Fig. 3c shows a ~0.4-km-deep TIL at ~1.8 km. A thick TIL hinders the upward transport of aerosols and facilitate the vertical mixing of N_{CCN} below the TIL. N_{CCN} thus varies little with altitude below the TIL, with a mean N_{CCN} at 0.7% *ss* of 5140 cm^{-3} (Fig. 3d). The θ profile in Fig. 3c suggests that $\partial\theta/\partial z$ above the TIL is much larger than below the TIL, meaning a more stable atmosphere above the TIL. N_{CCN} quickly decreases by an order of magnitude from below to above the TIL (from 5542 cm^{-3} at ~1.8 km to 365 cm^{-3} at ~2.2 km). Overall, the presence of a thick TIL has a large impact on the N_{CCN} profile.

Two TILs: The temperature profile in Fig. 3e depicts two shallow TILs with the same depth of ~0.2 km, appearing at ~0.8 km and ~2.5 km, respectively. Due to the hindering effect of a TIL on the vertical transport of aerosols, only a small amount of CCN break through the first TIL and diffuse to higher altitudes. Figure 3f suggests that N_{CCN} increases with altitude from near the surface to the bottom of the first TIL. A large amount of CCN accumulate below the first TIL, peaking at its bottom. The second TIL makes N_{CCN} accumulate again between the two TILs. Under the combined effect of two TILs, the upward transport of CCN becomes difficult. The θ profile in Fig. 3e also shows that $\partial\theta/\partial z$ is always positive, varying slightly with height. N_{CCN} generally experiences a declining trend with altitude between the two TILs (from 6380 cm^{-3} at 0.9 km to 635 cm^{-3} at 2.5 km). Above the second TIL, N_{CCN} remains at low and stable, with concentrations on the order of 10^2 cm^{-3}.

https://doi.org/10.5194/egusphere-2022-375
Preprint. Discussion started: 30 May 2022

In summary, the TIL structure has an important impact on the vertical distribution of N_{CCN}. Moreover, N_{CCN} in the free troposphere are easily impacted by the long-distance transport of aerosols under the influence of northwest air masses.

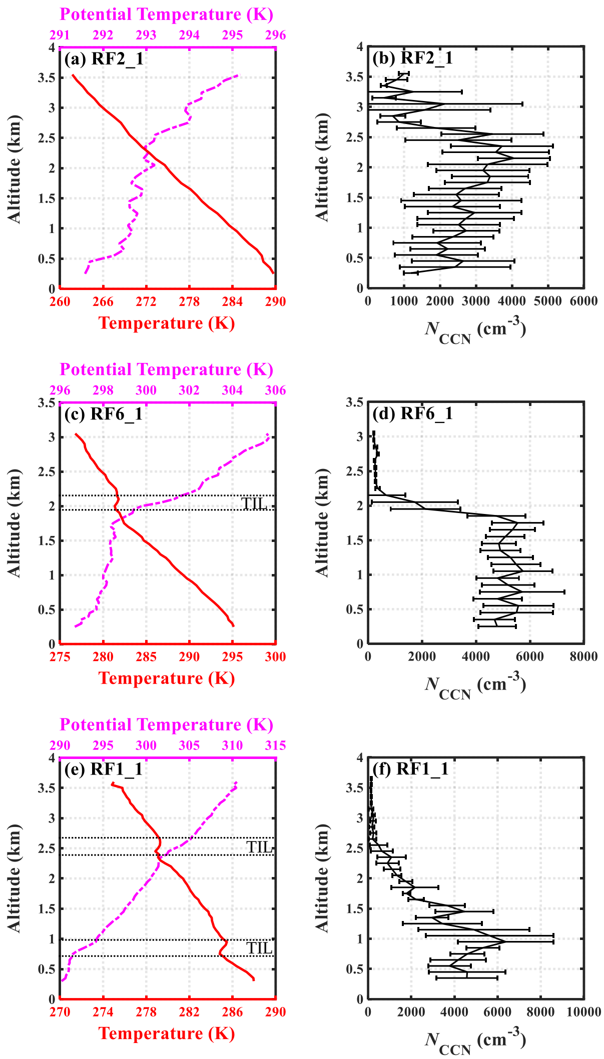

Figure 3. Vertical distributions of temperature (*T*) and potential temperature (θ) (**a, c, e**), and N_{CCN} at 0.7% *ss* (**b, d, f**) for RF2_1, RF6_1, and RF1_1 N_{CCN} profiles with (from top to bottom) no temperature inversion layer (TIL), one TIL, and two TILs. Horizontal error bars represent standard deviations of N_{CCN} at 0.7% *ss* at altitude intervals of 100 m.

https://doi.org/10.5194/egusphere-2022-375
Preprint. Discussion started: 30 May 2022

3.1.2 Influence of air masses on N_{CCN} profiles

To further investigate the influence of air masses on N_{CCN} profiles, the mean N_{CCN} at 0.7% *ss* in different altitude ranges in two distinct air masses is analyzed (Fig. 4). In general, the mean N_{CCN} at 0.7% *ss* has a declining trend with increasing altitude in both air masses (Fig. 4a). The N_{CCN} in southeast air masses is higher than in northwest air masses below 1.5 km, indicating more aerosol particles that can be activated as CCN in southeast air masses. Section 2.3 indicates that southeast air masses always pass over the densely populated plain area. This means that massive anthropogenic emissions can clearly increase N_{CCN} near the surface. However, N_{CCN} above 2 km is much lower in southeast air masses than in northwest air masses. This further indicates that the long-range transport of aerosols under the influence of northwest air masses contributes significantly to N_{CCN} in the free troposphere.

Figures 4b and 4c depict the mean N_{CCN} at 0.7% *ss* in different altitude ranges in northwest and southeast air masses, respectively. Under the influence of northwest air masses, the temperature structure varies, leading to different N_{CCN} profiles (Fig. 4b). For RF2_1 and RF2_2 N_{CCN} profiles with no TIL (Figs. 3b and S2b), the combined effect of upward and long-distance transport of aerosols increases N_{CCN} at 0.7% *ss* above 2 km. The N_{CCN} from 2 to 2.5 km is even higher than near the surface. For the RF11_1 N_{CCN} profile with one TIL, N_{CCN} at 0.7% *ss* varies slightly with altitude. For RF1_1 and RF1_2 N_{CCN} profiles with two TILs, N_{CCN} at 0.7% *ss* above 2 km is much lower than near the surface.

Under the influence of southeast air masses, the thermal structure for all N_{CCN} profiles is similar, with one TIL (Table 3). The N_{CCN} profile patterns are thus similar, showing much lower N_{CCN} above 2 km than near the surface (Fig. 4c). Figure 4c also suggests that N_{CCN} at 0.7% *ss* below 2 km is higher in the RF6_1 and RF6_2 N_{CCN} profiles than in the other three N_{CCN} profiles (i.e., RF7_1, RF7_2, and RF8_1). As discussed in section 2.3, air masses during RF6_1 and RF6_2 originate from the western Pacific, while the others originate from coastal areas. This suggests that the impact of marine aerosols is the possible reason for high N_{CCN} in the RF6_1 and RF6_2 N_{CCN} profiles. Figure 4c also shows that the N_{CCN} below 2 km is much higher at XT than at QZ and JL during the same flights (RF6_2 vs. RF6_1, and RF7_1 vs. RF7_2). Figure 1b shows that the XT site is closer

https://doi.org/10.5194/egusphere-2022-375
Preprint. Discussion started: 30 May 2022

to the Taihang Mountains than the QZ and JL sites. This implies that the terrain blocking effect of the Taihang Mountains on aerosols accumulates aerosols, resulting in higher N_{CCN} at XT.

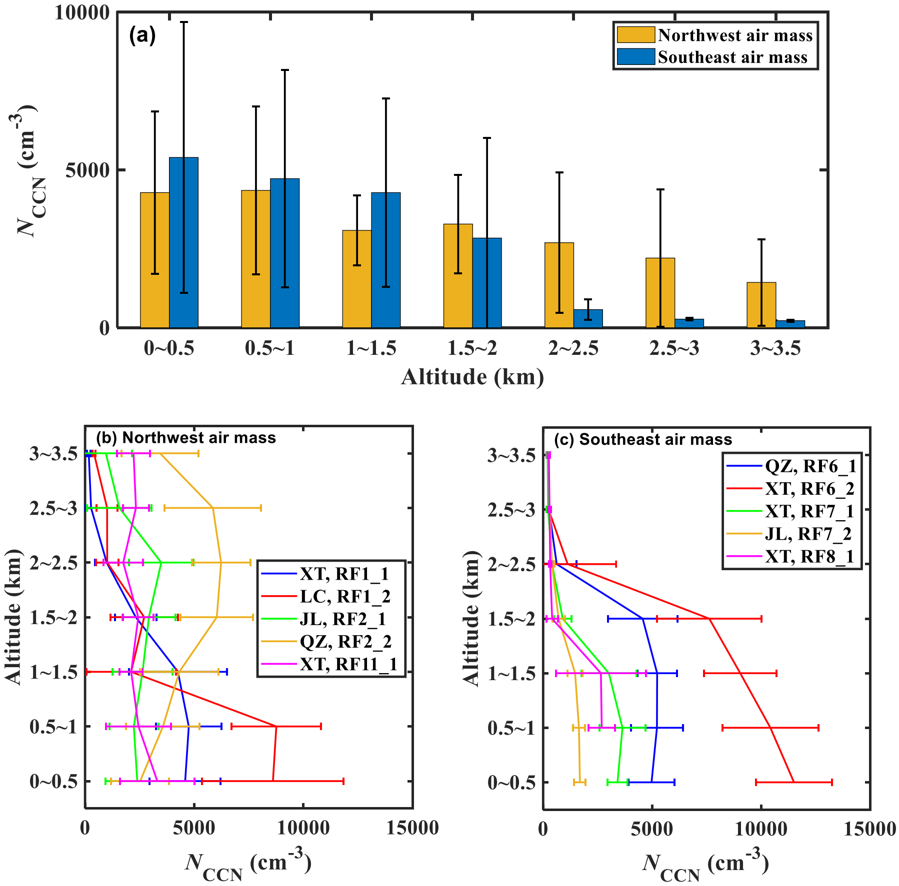

Figure 4. (a) Mean N_{CCN} at 0.7% *ss* in different altitude ranges (ranging from 0 to 3.5 km at intervals of 0.5 km) in northwest and southeast air masses, and for different N_{CCN} profiles at 0.7% *ss* in **(b)** northwest air masses and **(c)** southeast air masses. The different colors in (b) and (c) are for different flights. Error bars represent standard deviations of N_{CCN} at 0.7% *ss*.

In summary, N_{CCN} profiles *ss* are influenced by multiple factors over the NCP. TIL structure, aerosol long-range transport, and anthropogenic emissions lead to differences in the N_{CCN} profiles in different air masses. Even in the same air mass, diverse aerosol sources and terrain distributions cause large differences in N_{CCN}.

https://doi.org/10.5194/egusphere-2022-375
Preprint. Discussion started: 30 May 2022

3.2 Vertical distributions of CCN spectra in different air masses

The CCN spectrum is usually defined as a function of N_{CCN} to *ss*. Twomey (1959) first reported that N_{CCN} had an exponential relationship with *ss*. Since then, a variety of such functions have been proposed thanks to a large number of observations made which are all necessary given its nature of empirical relationships whose validity are generally limited. For example, Ji and Shaw (1998) provided a three-parameter function, while Gunthe et al. (2011) suggested a logarithmic function to fit CCN spectra. In this study, N_{CCN} measurements made at different *ss* during 11 level fights are used to fit CCN spectra. Twomey's relation (Twomey, 1959; Cohard et al., 1998) is used to fit the relationship between N_{CCN} and *ss* according to the least-squares method:

$$N_{\mathrm{CCN}}(ss) = C \bullet (ss)^{k} \qquad (1)$$

where $N_{\mathrm{CCN}}(ss)$ is the N_{CCN} at a specified *ss*, and *C* and *k* are two fitting coefficients. Table S1 lists the fitting results for the 11 level flights. In Eq. (1), the *C* value represents N_{CCN} at 1.0% *ss*, and the shape of the CCN spectrum is determined by the *k* value. Previous studies have suggested that *k* is closely related to the shape of particle number size distribution (PNSD) and aerosol hygroscopicity (e.g., Hegg et al., 1991; Jefferson, 2010). A lower *k* value means a stronger aerosol activation ability (i.e., more coarse-mode particles or stronger aerosol hygroscopicity), and vice versa.

Figure 5 shows CCN spectra at different altitudes during three level flights (RF2, RF6, and RF7). The seventy-two-hour back trajectories (Fig. 2a) suggest that the RF2 flight is influenced by northwest air masses. The CCN spectra during three level flights (RF2_a, RF2_b, and RF2_c; Fig. 5a) shows that *C* and *k* are lower at 3.6 km (RF2_b) than at 0.4 km (RF2_a and RF2_c), indicating smaller N_{CCN} but stronger aerosol activation ability in the free atmosphere than near the surface. At the same altitude (0.4 km), *C* during the RF2_c flight (6560 cm^{-3}) is more than two times that during the RF2_a flight (3029 cm^{-3}), with different *k* values (1.75 and 1.71, respectively). This indicates the regional variation of N_{CCN} and the weak aerosol activation ability near the surface.

Figures 5b and 5c show CCN spectra during flights RF6 and RF7, which are influenced by southeast air masses (Fig. 2b). The *k* values associated with southeast air masses (Fig. 5b and 5c) are always lower than those associated with northwest air masses (Fig. 5a). Therefore, aerosols in southeast air masses have a stronger activation ability than those in northwest air masses. This is likely because aerosols from southeast are mostly from anthropogenic emissions including more secondary particle matters such as sulfate and nitrate, while from northwest contains more natural

https://doi.org/10.5194/egusphere-2022-375
Preprint. Discussion started: 30 May 2022

components such as mineral dust (Xia et al., 2019; Q. Wang et al., 2022). Figure 5c also shows that *k* during the RF7 flight decreases from 0.65 at 0.4 km to 0.37 at 1.8 km, increasing to 0.62 at 3.1 km. Figures S3c and S3e show that the altitude of the TIL during the RF7 flight is ~2 km. This suggests that the aerosol activation ability near the TIL is stronger than that near the surface and in the free atmosphere above the TIL. This implies that the hindering effect of the TIL promotes aerosol aging processes, enhancing the aerosol activation ability (Y. Wang et al., 2018).

Overall, CCN spectra clearly varies with altitude over the NCP. The fitting coefficients of CCN spectra (*C* and *k*) are closely related to air mass sources, regional aerosol properties, and temperature structure.

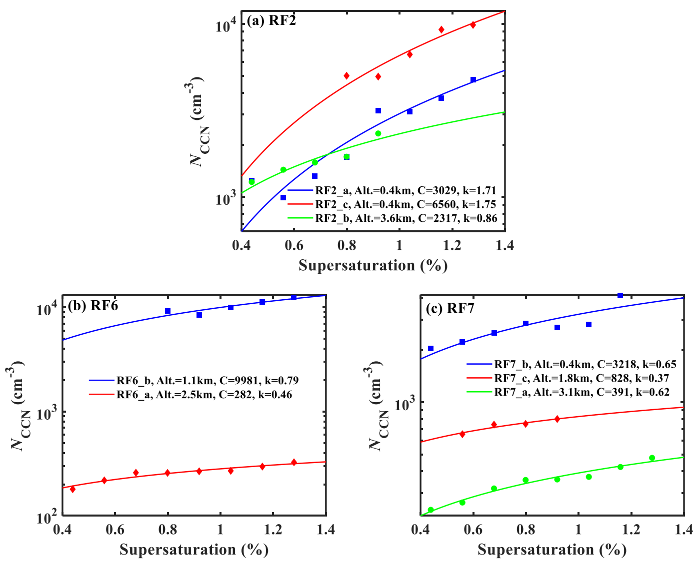

Figure 5. Fitted CCN spectra at different altitudes during three flights: (**a**) RF2, (**b**) RF6, and (**c**) RF7. The flight code, flight altitude (Alt.), and the two fitting coefficients from Twomey's relation (*C* and *k*) are given in each panel. Solid lines are the fitting lines described by Eq. (1).

3.3 The relationship between N_{CCN} and aerosol optical properties

3.3.1 Vertical distributions of aerosol scattering Ångström exponent (SAE)

The SAE is calculated as follows, where $\sigma(\lambda 1)$ and $\sigma(\lambda 2)$ are aerosol scattering coefficients at two given wavelengths (λ_1 = 450 nm and λ_2 = 700 nm)

https://doi.org/10.5194/egusphere-2022-375
Preprint. Discussion started: 30 May 2022

$$\mathrm{SAE} = -\frac{\log(\sigma(\lambda_1)) - \log(\sigma(\lambda_2))}{\log(\lambda_1) - \log(\lambda_2)} \qquad (2)$$

SAE is often used to qualitatively assess the dominant size mode of aerosols, reflecting the PNSD pattern (e.g., Hamonou et al., 1999). A large SAE (> 2) generally implies that fine-mode aerosols dominated (e.g., smoke particles), while a small SAE (< 1) means that the coarse mode dominated (e.g., dust particles).

Figure 6a shows the vertical distributions of SAE during the vertical spiral flights. Three profiles (RF2_1, RF2_2, and RF11_1) are not shown due to the lack of aerosol optical data. In general, SAE decreases gradually with altitude, while its standard deviation increases with altitude. This is likely because aerosols near the surface are easily influenced by primary emissions from anthropogenic sources, consisting of more fine particles. The frequent appearance of a TIL at ~2 km suppresses the upward transport of fine particles, leading to the rapid decrease of SAE above the TIL. The long-distance transport of coarse-mode aerosols (like dust particles) also decreases SAE in the free troposphere. As mentioned before, aerosol sources above 2 km are complex, which is why the standard deviation of SAE is larger above ~2 km.

Figure 6b shows profiles of N_{CCN} and σ (data used here were collected at 0.7% *ss* and 450 nm, respectively) during the RF1_1 spiral flight. Figure S5 shows profiles from the other spiral flights. In general, the vertical variation of σ is synchronous with that of N_{CCN}, indicating that they are correlated to some degree.

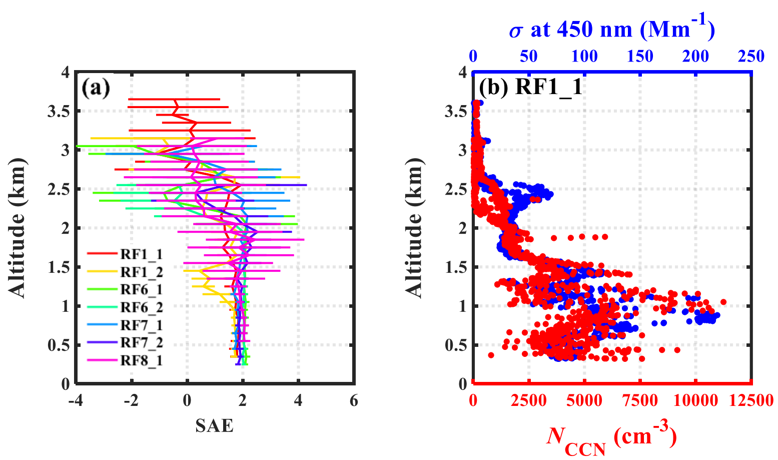

Figure 6. Vertical distributions of (**a**) aerosol scattering Ångström exponent (SAE) during the vertical spiral flights (error bars are standard deviations of SAE) and (**b**) N_{CCN} at 0.7% *ss* (red dots)

https://doi.org/10.5194/egusphere-2022-375
Preprint. Discussion started: 30 May 2022

and aerosol scattering coefficient (σ) at 450 nm (blue dots) during the RF1_1 vertical spiral flight.

3.3.2 Estimation of NCCN from aerosol optical properties

Both N_{CCN} and aerosol optical properties are affected by the same factors (e.g., PNSD and chemical composition). Therefore, numerous studies attempted to estimate N_{CCN} for aerosol optical properties, although there was no directly physical connection between them (e.g., Andreae, 2009; Liu and Li, 2014; Tao et al., 2018). Previous studies indicated that the relationship between N_{CCN} and σ was non-linear, mainly due to the variation of PNSD patterns (e.g., Andreae, 2009; Shinozuka et al., 2015). As discussed in section 3.3.1, SAE can be used to reflect the PNSD pattern. The clear vertical variation of SAE (Fig. 6a) suggests a complex and variable relationship between N_{CCN} at 0.7% *ss* and σ at 450 nm at different altitudes. Here, the parameterization provided by Shinozuka et al. (2015) is used:

$$N_{\mathrm{CCN}}=10^{\beta}\cdot\sigma^{\gamma} \tag{3}$$

where σ is the aerosol scattering coefficient at 450 nm, and β and γ are two fitting parameters. Shinozuka et al. (2015) suggested that β and γ were correlated to SAE, but the degree of correlation differed in different regions. In this study, N_{CCN} at 0.7% *ss* and SAE data points are paired to derive β and γ. N_{CCN} at other *ss* levels are too little to do this work because of the loop measurement of different *ss* levels in the second column of CCNc-200.

Figure 7 shows the relationships between SAE and β and SAE and γ in two air masses. β is negatively correlated with SAE, while γ is positively correlated with SAE. The correlations are lower (smaller coefficients of determination, R^2) in northwest air masses than in southeast air masses, likely due to more complex aerosol sources in northwest air masses. Empirical estimates of N_{CCN} at 0.7% *ss* from aerosol optical properties are determined as follows:

$$\text{Northwest air mass:}\quad N_{\mathrm{CCN}}=10^{-0.22\cdot\mathrm{SAE}+2.39}\cdot\sigma^{0.30\cdot\mathrm{SAE}+0.29} \tag{4}$$

$$\text{Southeast air mass:}\quad N_{\mathrm{CCN}}=10^{-0.07\cdot\mathrm{SAE}+2.29}\cdot\sigma^{0.14\cdot\mathrm{SAE}+0.28} \tag{5}$$

https://doi.org/10.5194/egusphere-2022-375
Preprint. Discussion started: 30 May 2022

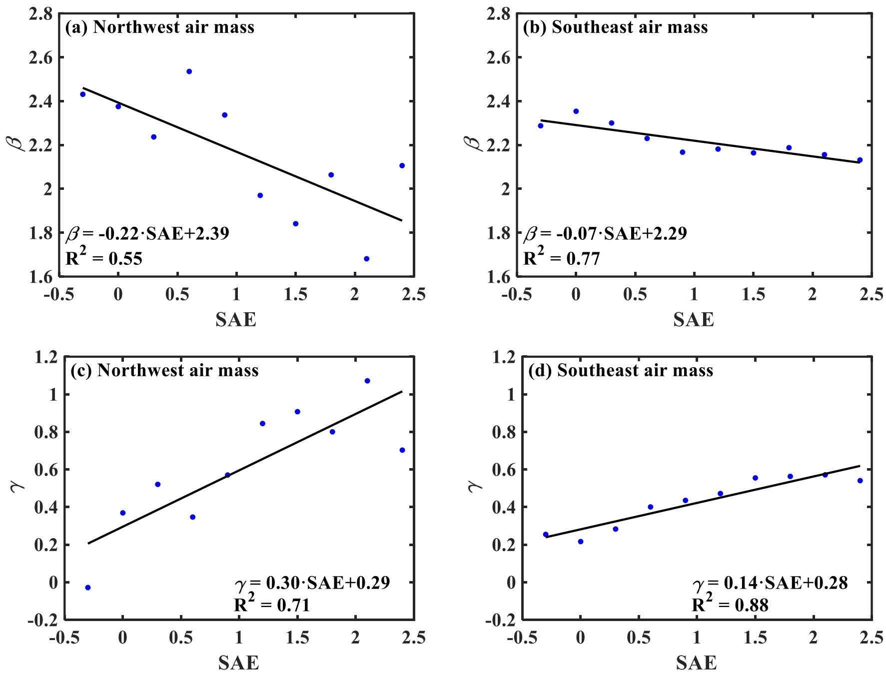

Figure 7. The two fitting parameters β and γ as a function of the aerosol scattering Ångström exponent (SAE) in northwest air masses (**a** and **c**) and southeast air masses (**b** and **d**). The dots are mean values averaged in 0.3-wide SAE bins. The black lines are best-fit lines from linear regression. Linear relations and coefficients of determination are given in each panel.

Figure 8 shows the comparisons of measured N_{CCN} at 0.7% *ss* and estimated N_{CCN} at 0.7% *ss* using Eqs. (4) and (5) for different vertical spiral flights in northwest and southwest air masses. For both air masses, most points approach the 1:1 line, indicating reasonable estimates using Eq. (4) and (5) to parameterize N_{CCN}. For northwest air masses (Fig. 8a), N_{CCN} estimates are better under high concentration conditions than under low concentration conditions. However, for southeast air masses, N_{CCN} estimates are better under low concentration conditions than under high concentration conditions. This is likely related to various aerosol sources at different altitudes. As previously discussed, most low N_{CCN} values are observed in the upper atmosphere above the TIL, while high N_{CCN} values are observed below the TIL. In northwest air masses, aerosol sources in the upper atmosphere are diverse, including the upward and long-distance transport of aerosols. This is why N_{CCN} estimates worsen under low N_{CCN} conditions. In southeast air masses, a single but thick TIL makes most aerosols accumulate in the lower atmosphere, where local emissions and the impact of

https://doi.org/10.5194/egusphere-2022-375
Preprint. Discussion started: 30 May 2022

marine aerosols exacerbate N_{CCN} estimates. These results highlight the important impact of aerosol sources on the empirical estimate of N_{CCN} from aerosol optical properties.

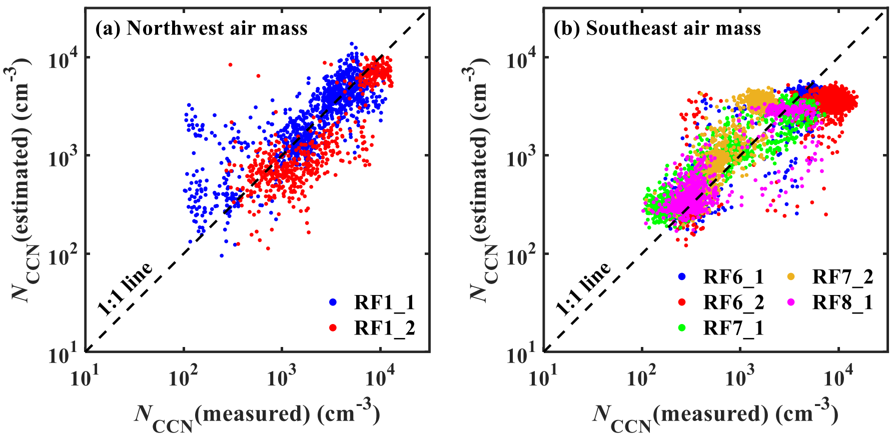

Figure 8. Comparisons between measured N_{CCN} at 0.7% *ss* and estimated N_{CCN} at 0.7% *ss* using Eqs. (4) and (5) for different vertical spiral flights in (**a**) northwest and (**b**) southeast air masses.

4. Conclusions

A comprehensive airborne campaign was conducted over the North China Plain (NCP) under the aegis of a project called Air chemistry Research In Asia (ARIAs). Seventy-two-hour air mass back trajectories show that the region of study during this campaign is mainly influenced by northwest and southeast air masses, originating from arid/semi-arid regions and coastal or marine areas, respectively. In this study, the profiles of cloud condensation nuclei number concentration (N_{CCN}) and their estimates from aerosol optical properties are analyzed.

It is found that N_{CCN} profiles at the water vapor supersaturation (*ss*) of 0.7% are impacted largely by the temperature structure in the atmosphere. In general, the presence of a temperature inversion layer (TIL) suppresses the upward transport of aerosols from near the surface, which is affected by the number and thickness of TILs. In addition, air mass sources have a significant impact on N_{CCN} profile characteristics. Under the influence of northwest air masses, N_{CCN} in the free troposphere are easily impacted by the long-distance transport of aerosols. However, under the influence of southeast air masses, atmospheric thermal structures for all N_{CCN} profiles are similar,

https://doi.org/10.5194/egusphere-2022-375
Preprint. Discussion started: 30 May 2022

with one TIL present in all cases. The patterns of N_{CCN} profiles are also similar, showing much lower N_{CCN} above the TIL than near the surface. In addition to the impact of anthropogenic emissions, the transport of marine aerosols is another reason for the high N_{CCN} near the surface when a southeast air mass is present. Moreover, comparisons of N_{CCN} profiles during the same flights suggests that the terrain blocking effect of the Taihang Mountains on aerosols accumulates aerosols, resulting in high N_{CCN} near the mountains.

The Twomey's relation ($N_{CCN}(ss) = C \bullet (ss)^k$, where C and k are two fitting coefficients) is used to analyze CCN spectra and aerosol activation ability in this study. In general, there is a clear change in CCN spectra with altitude. The aerosol activation ability in southeast air masses is stronger than in northwest air masses, mainly due to the different chemical composition associated with diverse air masses. In addition, the aerosol activation ability is stronger in the free atmosphere than near the surface. The hindering effect of a TIL on the upward transport of aerosols promotes aerosol aging processes, enhancing the aerosol activation ability near the TIL. The vertical distribution of aerosol scattering Ångström exponent (SAE) indicates that aerosols near the surface are easily influenced by primary emissions, consisting of more fine particles. The combined effect of aerosol upward and long-distance transport increases SAE and make it vary more in the free troposphere than near the surface.

The comparison of N_{CCN} at 0.7% ss and aerosol scattering coefficient (σ) at 450 nm suggests that the vertical variation of σ is synchronous with that of N_{CCN}. The equation, $N_{CCN}=10^{\beta}\cdot\sigma^{\gamma}$ (β and γ are two fitting parameters), is used to parameterize N_{CCN}, with the parameters β and γ being linearly correlated with the SAE. Empirical estimates of N_{CCN} at 0.7% ss from aerosol optical properties are thus retrieved ($N_{CCN}=10^{-0.22\cdot SAE+2.39}\cdot\sigma^{0.30\cdot SAE+0.29}$ for northwest air masses, and $N_{CCN}=10^{-0.07\cdot SAE+2.29}\cdot\sigma^{0.14\cdot SAE+0.28}$ for southeast air masses). The closure between the estimated and measured N_{CCN} at 0.7% ss is acceptable although different performances are seen under low and high concentration conditions for the two air masses. Results suggest the important impact of aerosol sources on the empirical estimate of N_{CCN} from aerosol optical properties.

N_{CCN} profiles in the NCP are impacted by multiple factors, including temperature structure, air mass sources, anthropogenic emissions, and terrain distribution. These factors make estimating N_{CCN} from aerosol optical properties more difficult. In the future, more aircraft measurement data will be needed to establish a more reasonable parameterization scheme for N_{CCN} at different ss. This

https://doi.org/10.5194/egusphere-2022-375
Preprint. Discussion started: 30 May 2022

study may also be useful for studying aerosol activation ability in other regions of the world.

Acknowledgements. This work was funded by the National Natural Science Foundation of China (NSFC) research project (grant nos. 42005067 and 42030606), the National Science Foundation of the United States (grant no. 1558259). We also thank all participants in the campaign for their tireless work and cooperation, especially the work of the Hebei Weather Modification Office.

Data availability. Measurement data from the field campaign used in this study are available from the corresponding author upon request (yuyingwang@nuist.edu.cn).

Author contributions. ZL and YW determined the main goal of this study. RZ and YW conceived the study and prepared this paper. ZL, RD, HS, and YC led the airborne campaign, ZW, XR, HH, and FW conducted this airborne campaign. HS, YC, and ZW provided the CCN data. YG, XC, and JX processed the measurement data. All co-authors participated in science discussions and suggested analyses.

Competing interests. The authors declare that they have no conflict of interest.

5. References

Anderson, T. L. and Ogren, J. A.: Determining aerosol radiative properties using the TSI 3563 integrating nephelometer, Aerosol Science and Technology, 29, 57-69, https://doi.org/10.1080/02786829808965551, 1998.

Andreae, M. O.: Correlation between cloud condensation nuclei concentration and aerosol optical thickness in remote and polluted regions, Atmospheric Chemistry and Physics, 9, 543-556, https://doi.org/10.5194/acp-9-543-2009, 2009.

Andreae, M. O. and Rosenfeld, D.: Aerosol–cloud–precipitation interactions. Part 1. The nature and sources of cloud-active aerosols, Earth-Science Reviews, 89, 13-41, https://doi.org/10.1016/j.earscirev.2008.03.001, 2008.

Bond, T. C., Doherty, S. J., Fahey, D. W., Forster, P. M., Berntsen, T., DeAngelo, B. J., Flanner, M. G., Ghan, S., Kärcher, B., Koch, D., Kinne, S., Kondo, Y., Quinn, P. K., Sarofim, M. C., Schultz, M. G., Schulz, M., Venkataraman, C., Zhang, H., Zhang, S., Bellouin, N., Guttikunda, S. K., Hopke, P. K., Jacobson, M. Z., Kaiser, J. W., Klimont, Z., Lohmann, U., Schwarz, J. P., Shindell, D., Storelvmo, T., Warren, S. G., and Zender, C. S.: Bounding the role of black carbon in the climate system: A scientific assessment, Journal of Geophysical Research: Atmospheres, 118, 5380-5552,

https://doi.org/10.5194/egusphere-2022-375
Preprint. Discussion started: 30 May 2022

https://doi.org/10.1002/jgrd.50171, 2013.

Cai, M., Tan, H., Chan, C. K., Qin, Y., Xu, H., Li, F., Schurman, M. I., Liu, L., and Zhao, J.: The size-resolved cloud condensation nuclei (CCN) activity and its prediction based on aerosol hygroscopicity and composition in the Pearl Delta River (PRD) region during wintertime 2014, Atmospheric Chemistry and Physics, 18, 16,419-16,437, https://doi.org/10.5194/acp-18-16419-2018, 2018.

Cai, Z., Li, Z., Li, P., Li, J., Sun, H., Yang, Y., Gao, X., Ren, G., Ren, R., and Wei, J.: Vertical distributions of aerosol microphysical and optical properties based on aircraft measurements made over the Loess Plateau in China, Atmospheric Environment, 270, 118888, https://doi.org/10.1016/j.atmosenv.2021.118888, 2022.

Chen, C., Qiu, Y., Xu, W., He, Y., Li, Z., Sun, J., Ma, N., Xu, W., Pan, X., Fu, P., Wang, Z., and Sun, Y.: Primary emissions and secondary aerosol processing during wintertime in rural area of North China Plain, Journal of Geophysical Research: Atmospheres, 127, e2021JD035430, https://doi.org/10.1029/2021JD035430, 2022.

Cohard, J.-M., Pinty, J.-P., and Bedos, C.: Extending Twomey's analytical estimate of nucleated cloud droplet concentrations from CCN spectra, Journal of the Atmospheric Sciences, 55, 3348-3357, https://doi.org/10.1175/1520-0469(1998)055<3348:Etsaeo>2.0.Co;2, 1998.

Draxier, R. R. and Hess, G. D.: An overview of the HYSPLIT_4 modeling system of trajectories, dispersion, and deposition, Australian Meteorological Magazine, 47, 295-308, 1998.

Fan, J., Wang, Y., Rosenfeld, D., and Liu, X.: Review of aerosol–cloud interactions: mechanisms, significance, and challenges, Journal of the Atmospheric Sciences, 73, 4221-4252, https://doi.org/10.1175/jas-d-16-0037.1, 2016.

Farmer, D. K., Cappa, C. D., and Kreidenweis, S. M.: Atmospheric processes and their controlling influence on cloud condensation nuclei activity, Chemical Reviews, 115, 4199-4217, https://doi.org/10.1021/cr5006292, 2015.

Gunthe, S. S., Rose, D., Su, H., Garland, R. M., Achtert, P., Nowak, A., Wiedensohler, A., Kuwata, M., Takegawa, N., Kondo, Y., Hu, M., Shao, M., Zhu, T., Andreae, M. O., and Pöschl, U.: Cloud condensation nuclei (CCN) from fresh and aged air pollution in the megacity region of Beijing, Atmospheric Chemistry and Physics, 11, 11,023-11,039, https://doi.org/10.5194/acp-11-11023-2011, 2011.

Guo, L. J., Guo, X. L., Fang, C. G., and Zhu, S. C.: Observation analysis on characteristics of formation, evolution and transition of a long-lasting severe fog and haze episode in North China, Science China-Earth Sciences, 58, 329-344, https://doi.org/10.1007/s11430-014-4924-2, 2015.

Hamonou, E., Chazette, P., Balis, D., Dulac, F., Schneider, X., Galani, E., Ancellet, G., and Papayannis, A.: Characterization of the vertical structure of Saharan dust export to the Mediterranean basin, Journal of Geophysical Research: Atmospheres, 104, 22,257-22,270, https://doi.org/10.1029/1999jd900257, 1999.

Hegg, D. A., Radke, L. F., and Hobbs, P. V.: Measurements of Aitken nuclei and cloud condensation nuclei in the marine atmosphere and their relation to the DMS-Cloud-climate hypothesis, Journal of Geophysical Research: Atmospheres, 96, 18,727-18,733, https://doi.org/10.1029/91JD01870, 1991.

IPCC. Climate Change 2021: The physical basis, sixth assessment of the Inter-governmental Panel on Climate Change[M]. Cambridge University Press, 2021.

Janhäll, S., Olofson, K. F. G., Andersson, P. U., Pettersson, J. B. C., and Hallquist, M.: Evolution of the

https://doi.org/10.5194/egusphere-2022-375
Preprint. Discussion started: 30 May 2022

urban aerosol during winter temperature inversion episodes, Atmospheric Environment, 40, 5355-5366, https://doi.org/10.1016/j.atmosenv.2006.04.051, 2006.

Jayachandran, V. N., Suresh Babu, S. N., Vaishya, A., Gogoi, M. M., Nair, V. S., Satheesh, S. K., and Krishna Moorthy, K.: Altitude profiles of cloud condensation nuclei characteristics across the Indo-Gangetic Plain prior to the onset of the Indian summer monsoon, Atmospheric Chemistry and Physics, 20, 561-576, https://doi.org/10.5194/acp-20-561-2020, 2020a.

Jayachandran, V. N., Varghese, M., Murugavel, P., Todekar, K. S., Bankar, S. P., Malap, N., Dinesh, G., Safai, P. D., Rao, J., Konwar, M., Dixit, S., and Prabha, T. V.: Cloud condensation nuclei characteristics during the Indian summer monsoon over a rain-shadow region, Atmospheric Chemistry and Physics, 20, 7307-7334, https://doi.org/10.5194/acp-20-7307-2020, 2020b.

Jefferson, A.: Empirical estimates of CCN from aerosol optical properties at four remote sites, Atmos. Chem. Phys., 10, 6855-6861, https://doi.org/10.5194/acp-10-6855-2010, 2010.

Ji, Q. and Shaw, G. E.: On supersaturation spectrum and size distributions of cloud condensation nuclei, Geophysical Research Letters, 25, 1903-1906, https://doi.org/10.1029/98GL01404, 1998.

Juranyi, Z., Gysel, M., Weingartner, E., Bukowiecki, N., Kammermann, L., and Baltensperger, U.: A 17 month climatology of the cloud condensation nuclei number concentration at the high alpine site Jungfraujoch, Journal of Geophysical Research: Atmospheres, 116, https://doi.org/10.1029/2010JD015199, 2011.

Leng, C. P., Cheng, T. T., Chen, J. M., Zhang, R. J., Tao, J., Huang, G. H., Zha, S. P., Zhang, M. G., Fang, W., Li, X., and Li, L.: Measurements of surface cloud condensation nuclei and aerosol activity in downtown Shanghai, Atmospheric Environment, 69, 354-361, https://doi.org/10.1016/j.atmosenv.2012.12.021, 2013.

Li, J., Chen, H., Li, Z., Wang, P., Cribb, M., and Fan, X.: Low-level temperature inversions and their effect on aerosol condensation nuclei concentrations under different large-scale synoptic circulations, Advances in Atmospheric Sciences, 32, 898-908, https://doi.org/10.1007/s00376-014-4150-z, 2015a.

Li, J., Yin, Y., Li, P., Li, Z., Li, R., Cribb, M., Dong, Z., Zhang, F., Li, J., Ren, G., Jin, L., and Li, Y.: Aircraft measurements of the vertical distribution and activation property of aerosol particles over the Loess Plateau in China, Atmospheric Research, 155, 73-86, https://doi.org/10.1016/j.atmosres.2014.12.004, 2015b.

Li, Z., Lau, W. K.-M., Ramanathan, V., Wu, G., Ding, Y., Manoj, M. G., Liu, J., Qian, Y., Li, J., Zhou, T., Fan, J., Rosenfeld, D., Ming, Y., Wang, Y., Huang, J., Wang, B., Xu, X., Lee, S.-S., Cribb, M., Zhang, F., Yang, X., Zhao, C., Takemura, T., Wang, K., Xia, X., Yin, Y., Zhang, H., Guo, J., Zhai, P. M., Sugimoto, N., Babu, S. S., and Brasseur, G. P.: Aerosol and monsoon climate interactions over Asia, Reviews of Geophysics, 54, 866-929, https://doi.org/10.1002/2015RG000500, 2016.

Li, Z., Wang, Y., Guo, J., Zhao, C., Cribb, M. C., Dong, X., Fan, J., Gong, D., Huang, J., Jiang, M., Jiang, Y., Lee, S. S., Li, H., Li, J., Liu, J., Qian, Y., Rosenfeld, D., Shan, S., Sun, Y., Wang, H., Xin, J., Yan, X., Yang, X., Yang, X.-Q., Zhang, F., and Zheng, Y.: East Asian Study of Tropospheric Aerosols and their Impact on Regional Clouds, Precipitation, and Climate (EAST-AIRCPC), Journal of Geophysical Research: Atmospheres, 124, 13,026-13,054, https://doi.org/10.1029/2019JD030758, 2019.

Liu, J. and Li, Z.: Estimation of cloud condensation nuclei concentration from aerosol optical quantities: influential factors and uncertainties, Atmospheric Chemistry and Physics, 14, 471-483, https://doi.org/10.5194/acp-14-471-2014, 2014.

Liu, L., Cheng, Y., Wang, S., Wei, C., Pöhlker, M. L., Pöhlker, C., Artaxo, P., Shrivastava, M., Andreae, M. O., Pöschl, U., and Su, H.: Impact of biomass burning aerosols on radiation, clouds, and precipitation over the Amazon: relative importance of aerosol–cloud and aerosol–radiation interactions, Atmospheric Chemistry and Physics, 20, 13283-13301, https://doi.org/10.5194/acp-20-13283-2020, 2020.

Lohmann, U. and Feichter, J.: Global indirect aerosol effects: a review, Atmospheric Chemistry and Physics, 5, 715-737, https://doi.org/10.5194/acp-5-715-2005, 2005.

Manoj, M. R., Satheesh, S. K., Moorthy, K. K., Trembath, J., and Coe, H.: Measurement report: Altitudinal variation of cloud condensation nuclei activation across the Indo-Gangetic Plain prior to monsoon onset and during peak monsoon periods: results from the SWAAMI field campaign, Atmospheric Chemistry and Physics, 21, 8979-8997, https://doi.org/10.5194/acp-21-8979-2021, 2021.

Paramonov, M., Kerminen, V. M., Gysel, M., Aalto, P. P., Andreae, M. O., Asmi, E., Baltensperger, U., Bougiatioti, A., Brus, D., Frank, G. P., Good, N., Gunthe, S. S., Hao, L., Irwin, M., Jaatinen, A., Juranyi, Z., King, S. M., Kortelainen, A., Kristensson, A., Lihavainen, H., Kulmala, M., Lohmann, U., Martin, S. T., McFiggans, G., Mihalopoulos, N., Nenes, A., O'Dowd, C. D., Ovadnevaite, J., Petaja, T., Poschl, U., Roberts, G. C., Rose, D., Svenningsson, B., Swietlicki, E., Weingartner, E., Whitehead, J., Wiedensohler, A., Wittbom, C., and Sierau, B.: A synthesis of cloud condensation nuclei counter (CCNC) measurements within the EUCAARI network, Atmospheric Chemistry and Physics, 15, 12,211-12,229, https://doi.org/10.5194/acp-15-12211-2015, 2015.

Ren, J., Zhang, F., Wang, Y., Collins, D., Fan, X., Jin, X., Xu, W., Sun, Y., Cribb, M., and Li, Z.: Using different assumptions of aerosol mixing state and chemical composition to predict CCN concentrations based on field measurements in urban Beijing, Atmospheric Chemistry and Physics, 18, 6907-6921, https://doi.org/10.5194/acp-18-6907-2018, 2018.

Ren, R., Li, Z., Yan, P., Wang, Y., Wu, H., Cribb, M., Wang, W., Jin, X., Li, Y., and Zhang, D.: Measurement report: The effect of aerosol chemical composition on light scattering due to the hygroscopic swelling effect, Atmospheric Chemistry and Physics, 21, 9977-9994, https://doi.org/10.5194/acp-21-9977-2021, 2021.

Rose, D., Gunthe, S. S., Mikhailov, E., Frank, G. P., Dusek, U., Andreae, M. O., and Pöschl, U.: Calibration and measurement uncertainties of a continuous-flow cloud condensation nuclei counter (DMT-CCNC): CCN activation of ammonium sulfate and sodium chloride aerosol particles in theory and experiment, Atmospheric Chemistry and Physics, 8, 1153-1179, https://doi.org/10.5194/acp-8-1153-2008, 2008.

Rose, D., Nowak, A., Achtert, P., Wiedensohler, A., Hu, M., Shao, M., Zhang, Y., Andreae, M. O., and Pöschl, U.: Cloud condensation nuclei in polluted air and biomass burning smoke near the mega-city Guangzhou, China – Part 1: Size-resolved measurements and implications for the modeling of aerosol particle hygroscopicity and CCN activity, Atmospheric Chemistry and Physics, 10, 3365-3383, https://doi.org/10.5194/acp-10-3365-2010, 2010.

Rosenfeld, D., Lohmann, U., Raga, G. B., O'Dowd, C. D., Kulmala, M., Fuzzi, S., Reissell, A., and Andreae, M. O.: Flood or drought: How do aerosols affect precipitation?, Science, 321, 1309-1313, https://doi.org/10.1126/science.1160606, 2008.

Rosenfeld, D., Sherwood, S., Wood, R., and Donner, L.: Climate effects of aerosol-cloud interactions, Science, 343, 379-380, https://doi.org/10.1126/science.1247490, 2014.

Rosenfeld, D., Zheng, Y., Hashimshoni, E., Pöhlker, M. L., Jefferson, A., Pöhlker, C., Yu, X., Zhu, Y., Liu, G., Yue, Z., Fischman, B., Li, Z., Giguzin, D., Goren, T., Artaxo, P., Barbosa, H. M. J., Pöschl, U., and Andreae, M. O.: Satellite retrieval of cloud condensation nuclei concentrations by using clouds as CCN chambers, Proceedings of the National Academy of Sciences USA, 113, 5828-5834, https://doi.org/10.1073/pnas.1514044113, 2016.

Schmale, J., Henning, S., Decesari, S., Henzing, B., Keskinen, H., Sellegri, K., Ovadnevaite, J., Pohlker, M. L., Brito, J., Bougiatioti, A., Kristensson, A., Kalivitis, N., Stavroulas, I., Carbone, S., Jefferson, A., Park, M., Schlag, P., Iwamoto, Y., Aalto, P., Aijala, M., Bukowiecki, N., Ehn, M., Frank, G., Frohlich, R., Frumau, A., Herrmann, E., Herrmann, H., Holzinger, R., Kos, G., Kulmala, M., Mihalopoulos, N., Nenes, A., O'Dowd, C., Petaja, T., Picard, D., Pohlker, C., Poschl, U., Poulain, L., Prevot, A. S. H., Swietlicki, E., Andreae, M. O., Artaxo, P., Wiedensohler, A., Ogren, J., Matsuki, A., Yum, S. S., Stratmann, F., Baltensperger, U., and Gysel, M.: Long-term cloud condensation nuclei number concentration, particle number size distribution and chemical composition measurements at regionally representative observatories, Atmospheric Chemistry and Physics, 18, 2853-2881, https://doi.org/10.5194/acp-18-2853-2018, 2018.

Shinozuka, Y., Clarke, A. D., Nenes, A., Jefferson, A., Wood, R., McNaughton, C. S., Ström, J., Tunved, P., Redemann, J., Thornhill, K. L., Moore, R. H., Lathem, T. L., Lin, J. J., and Yoon, Y. J.: The relationship between cloud condensation nuclei (CCN) concentration and light extinction of dried particles: indications of underlying aerosol processes and implications for satellite-based CCN estimates, Atmospheric Chemistry and Physics, 15, 7585-7604, https://doi.org/10.5194/acp-15-7585-2015, 2015.

Tao, J., Zhao, C., Kuang, Y., Zhao, G., Shen, C., Yu, Y., Bian, Y., and Xu, W.: A new method for calculating number concentrations of cloud condensation nuclei based on measurements of a three-wavelength humidified nephelometer system, Atmospheric Measurement Techniques, 11, 895-906, https://doi.org/10.5194/amt-11-895-2018, 2018.

Twomey, S.: The nuclei of natural cloud formation.Ppart II: The supersaturation in natural clouds and the variation of cloud droplet concentration, Geofisica pura e applicata, 43, 243-249, https://doi.org/10.1007/BF01993560, 1959.

Wang, F., Li, Z., Ren, X., Jiang, Q., He, H., Dickerson, R. R., Dong, X., and Lv, F.: Vertical distributions of aerosol optical properties during the spring 2016 ARIAs airborne campaign in the North China Plain, Atmospheric Chemistry and Physics, 18, 8995-9010, https://doi.org/10.5194/acp-18-8995-2018, 2018.

Wang, Q., Du, W., Sun, Y., Wang, Z., Tang, G., and Zhu, J.: Submicron-scale aerosol above the city canopy in Beijing in spring based on in-situ meteorological tower measurements, Atmospheric Research, 271, 106128, https://doi.org/10.1016/j.atmosres.2022.106128, 2022

Wang, Y., Li, Z., Zhang, Y., Du, W., Zhang, F., Tan, H., Xu, H., Fan, T., Jin, X., Fan, X., Dong, Z., Wang, Q., and Sun, Y.: Characterization of aerosol hygroscopicity, mixing state, and CCN activity at a suburban site in the central North China Plain, Atmospheric Chemistry and Physics, 18, 11,739-11,752, https://doi.org/10.5194/acp-18-11739-2018, 2018.

Xia, C., Sun, J., Qi, X., Shen, X., Zhong, J., Zhang, X., Wang, Y., Zhang, Y., and Hu, X.: Observational study of aerosol hygroscopic growth on scattering coefficient in Beijing: A case study in March of 2018, Science of The Total Environment, 685, 239-247, https://doi.org/10.1016/j.scitotenv.2019.05.283, 2019.

Xu, W., Ovadnevaite, J., Fossum, K. N., Lin, C. S., Huang, R. J., O'Dowd, C., and Ceburnis, D.: Aerosol hygroscopicity and its link to chemical composition in the coastal atmosphere of Mace Head: marine

https://doi.org/10.5194/egusphere-2022-375
Preprint. Discussion started: 30 May 2022

and continental air masses, Atmospheric Chemistry and Physics, 20, 3777-3791, https://doi.org/10.5194/acp-20-3777-2020, 2020.

Yau, M. K., and Rogers, R. R.: A short course in cloud physics, edited, Elsevier, 1996.

Zhang, F., Li, Z. Q., Li, Y. A., Sun, Y. L., Wang, Z. Z., Li, P., Sun, L., Wang, P. C., Cribb, M., Zhao, C. F., Fan, T. Y., Yang, X., and Wang, Q. Q.: Impacts of organic aerosols and its oxidation level on CCN activity from measurement at a suburban site in China, Atmospheric Chemistry and Physics, 16, 5413-5425, https://doi.org/10.5194/acp-16-5413-2016, 2016.

Zhang, F., Wang, Y. Y., Peng, J. F., Ren, J. Y., Collins, D., Zhang, R. Y., Sun, Y. L., Yang, X., and Li, Z. Q.: Uncertainty in predicting CCN activity of aged and primary aerosols, Journal of Geophysical Research: Atmospheres, 122, 11,723-11,736, https://doi.org/10.1002/2017jd027058, 2017.

Zhang, L., Sun, J. Y., Shen, X. J., Zhang, Y. M., Che, H., Ma, Q. L., Zhang, Y. W., Zhang, X. Y., and Ogren, J. A.: Observations of relative humidity effects on aerosol light scattering in the Yangtze River Delta of China, Atmospheric Chemistry and Physics, 15, 8439-8454, https://doi.org/10.5194/acp-15-8439-2015, 2015.